The Southern Ocean Overturning: Parameterized versus Permitted Eddies

PAUL SPENCE

School of Earth and Ocean Sciences, University of Victoria, Victoria, British Columbia, Canada

OLEG A. SAENKO

Canadian Centre for Climate Modelling and Analysis, Environment Canada, Victoria, British Columbia, Canada

MICHAEL EBY AND ANDREW J. WEAVER

School of Earth and Ocean Sciences, University of Victoria, Victoria, British Columbia, Canada

(Manuscript received 12 August 2008, in final form 15 January 2009)

ABSTRACT

Four versions of the same global climate model, with horizontal resolution ranging from 1.8° × 3.6° to 0.2° × 0.4°, are employed to evaluate the resolution dependence of the Southern Ocean meridional overturning circulation. At coarse resolutions North Atlantic Deep Water tends to upwell diabatically at low latitudes, so that the Southern Ocean is weakly coupled with the rest of the ocean. As resolution increases and eddy effects become less parameterized the interior circulation becomes more adiabatic and deep water increasingly upwells by flowing along isopycnals in the Southern Ocean, despite each model having the same vertical diffusivity profile. Separating the overturning circulation into mean and eddy-induced components demonstrates that both the permitted and the parameterized eddies induce overturning cells in the Southern Ocean with mass fluxes across mean isopycnals. It is found that for some density classes the transformation rate derived from surface buoyancy fluxes can provide a proxy for the net meridional transport in the upper Southern Ocean. Changes in the Southern Ocean overturning in response to poleward-intensifying Southern Hemisphere winds concomitant with increasing atmospheric CO_2 through the twenty-first century are also investigated. Results suggest that the circulation associated with the formation of Antarctic Intermediate Water is likely to strengthen, or stay essentially unchanged, rather than to slow down.

1. Introduction

The upper-ocean meridional overturning circulation (MOC) can be thought of as consisting of two branches (Gnanadesikan 1999). One is associated with deep-water formation in the northern North Atlantic where light waters are converted to dense waters. In the other branch, found in the Southern Ocean and in the low-latitude oceans, the reverse process takes place with dense water being converted back to light water. The two branches can influence each other in that, for example, a change in the dense-to-light water conversion in the Southern Ocean could translate into a change in the light-to-dense water conversion in the north, and vice versa. In models, the degree of this north–south connection may depend on the representation of the individual components of the MOC. In particular, coarse-resolution models that capture only the large-scale features of the circulation are obliged to parameterize the effects of unresolved mesoscale motions, that is, the motions that account for most of the kinetic energy in the ocean (e.g., Ducet et al. 2000; Wunsch 2007). In the Southern Ocean, where mesoscale eddies play a fundamental role in closing the MOC, there is a particular need to rely on such parameterizations.

One of the most, if not the most, widely employed schemes to parameterize the effect of mesoscale eddies on tracer transport and, hence, on large-scale circulation is that of Gent and McWilliams (1990, hereafter referred to as GM90). It has been shown in many studies that the GM90 scheme is capable of greatly improving the interior tracer distribution and can strongly influence the simulated MOC (e.g., Danabasoglu et al. 1994;

Corresponding author address: Paul Spence, School of Earth and Ocean Sciences, University of Victoria, P.O. Box 3055, Stn. CSC, Victoria, BC V8W 3P6, Canada.
E-mail: pspence@ocean.seos.uvic.ca

DOI: 10.1175/2009JPO4120.1

Wiebe and Weaver 1999). There are, however, unresolved questions. For example, Hallberg and Gnanadesikan (2006) question the ability of coarse-resolution models employing the GM90 scheme to accurately capture the impact of changes in the Southern Ocean winds on the MOC. Furthermore, Hirst and McDougall (1998) argue that it is not clear if the GM90 eddy-induced transport can actually be interpreted as a ''bolus'' transport arising from unresolved temporal correlations between varying isopycnal surfaces and velocities. They show in a coarse-resolution model that, while the GM90 eddy-induced transport could combine with ''resolved'' transport to produce a total (or residual) circulation that would tend to follow isopycnals in the interior, such a near-adiabatic nature of the circulation may not always hold for large-scale and eddy-induced flows separately. Thus, the eddy-induced circulation due to GM90 may lead to strong cross-isopycnal flows in coarse-resolution models (e.g., Hirst and McDougall 1998; Speer et al. 2000a; Saenko et al. 2005; see also Gent et al. 1995). Therefore, it remains unclear if the circulation induced by the parameterized eddies can be employed for tracking the pathways of the transport induced by ''permitted'' eddies. In addition, as resolution increases the simulated western boundary currents—an important component of the MOC—become less viscous, so that an input of vorticity due to the wind stress curl is expected to be mostly balanced by bottom pressure torques rather than by lateral viscous stresses (Hughes 2000). Furthermore, the influence of the subgrid-scale processes arising from convection and small-scale turbulent mixing may also depend on resolution. All these factors have the potential to produce substantial differences between simulations of the ocean circulation by coarse-resolution and eddy-permitting models, including such an integral quantity as the MOC.

The aim here is to employ four versions of the same model, ranging in horizontal resolution from coarse to (marginally) eddy permitting, in an attempt to understand how the simulated MOC depends on resolution. We will focus on the Southern Ocean and also try to connect the MOC to the local buoyancy input at the surface, following the approach first proposed by Walin (1982). We begin by discussing a theoretical framework for the meridional circulation and the transformation of Southern Ocean water masses (section 2). Section 3 describes the climate model we employ and the experimental design. The effect of increasing resolution on a near preindustrial (year 1900) control state of the MOC and transformation rates are analyzed in section 4. Section 5 evaluates their response to observed and projected poleward-intensifying Southern Hemisphere winds concomitant with increasing atmospheric CO_2 through the twenty-first century—a topic that is of major interest to the climate-modeling community (Fyfe et al. 2007; Treguier et al. 2007; Zickfeld et al. 2007). A discussion and conclusions are presented in section 6.

2. Theoretical framework

This section briefly describes some of the more recent theoretical developments linking the deep-water upwelling in the Southern Ocean and its transformation into lighter water to the surface fluxes of momentum and buoyancy. In the following sections, these theoretical ideas are used as a guide when analyzing the Southern Ocean overturning and the corresponding transformation rates simulated by a numerical model at different resolutions.

Since our focus is on the circulation in the meridional plane, it is relevant to consider a theory that assumes some kind of zonal averaging. In general, the issue of zonal averaging is important and not trivial. For example, one could apply zonal averaging along latitude circles; alternatively, it could be done along mean streamlines of the Antarctic Circumpolar Current (ACC) (e.g., Marshall and Radko 2003) or along mean buoyancy surfaces (e.g., Döös and Webb 1994), or both (Treguier et al. 2007). Each of these formulations has advantages and disadvantages. For example, the mean position of ACC is expected to vary with depth; whereas the isopycnal framework can be problematic near the surface where isopycnals outcrop in the presence of eddies. It is for the latter reason that the preference is often given to z coordinates (e.g., Plumb and Ferrari 2005), which is also taken here.

Following Karsten et al. (2002) and Marshall and Radko (2003), consider the steady buoyancy equation in the following form:

$$\overline{v}\frac{\partial \overline{b}}{\partial y} + \overline{w}\frac{\partial \overline{b}}{\partial z} + \frac{\partial}{\partial y}(\overline{v'b'}) + \frac{\partial}{\partial z}(\overline{w'b'}) = \frac{\partial B}{\partial z}, \qquad (1)$$

where $(\overline{v}, \overline{w})$ is the Eulerian mean velocity and $\overline{b}$ is the mean buoyancy and variables are separated into mean (zonal and time) quantities and perturbations from this mean; the term on the right-hand side represents diabatic processes due to small-scale mixing and, in the mixed layer, due to the surface buoyancy flux.

Introducing the slope of mean buoyancy surfaces, $s_\rho = -\overline{b}_y/\overline{b}_z$, it is convenient to decompose the eddy buoyancy flux $(\overline{v'b'}, \overline{w'b'})$ into an along-$\overline{b}$ component $(\overline{w'b'}/s_\rho, \overline{w'b'})$ and the remaining component $(\overline{v'b'} - \overline{w'b'}/s_\rho, 0)$. The divergence of the remaining component is the eddy contribution to the diabatic processes and is thought to be small below the mixed/diabatic layer,

whereas the divergence of the along-$\overline{b}$ component can be written as an advective transport:

$$\frac{\partial}{\partial y}\left(\frac{\overline{w'b'}}{s_\rho}\right) + \frac{\partial}{\partial z}(\overline{w'b'}) = -\frac{\partial}{\partial y}\left(\frac{\overline{w'b'}}{\partial_y \overline{b}}\right)\frac{\partial \overline{b}}{\partial z} + \frac{\partial}{\partial z}\left(\frac{\overline{w'b'}}{\partial_y \overline{b}}\right)\frac{\partial \overline{b}}{\partial y}, \quad (2)$$

or

$$\frac{\partial}{\partial y}\left(\frac{\overline{w'b'}}{s_\rho}\right) + \frac{\partial}{\partial z}(\overline{w'b'}) = +\frac{\partial \Psi^*}{\partial y}\frac{\partial \overline{b}}{\partial z} - \frac{\partial \Psi^*}{\partial z}\frac{\partial \overline{b}}{\partial y}, \quad (3)$$

where, as follows from Eq. (2), the eddy-induced streamfunction is given by

$$\Psi^* = -(\overline{w'b'})/\partial_y \overline{b}, \quad (4)$$

with the corresponding eddy transport velocity $(\upsilon^*, w^*) = (-\partial_z \Psi^*, \partial_y \Psi^*)$. Hence, Eq. (1) can be rewritten as follows:

$$(\overline{\upsilon} + \upsilon^*)\frac{\partial \overline{b}}{\partial y} + (\overline{w} + w^*)\frac{\partial \overline{b}}{\partial z} = \frac{\partial B}{\partial z} - \frac{\partial}{\partial y}\left(\overline{\upsilon'b'} - \frac{\overline{w'b'}}{s_\rho}\right). \quad (5)$$

Assuming that the Eulerian mean flow is nondivergent and introducing the corresponding streamfunction, $(\overline{\upsilon}, \overline{w}) = (-\partial_z \overline{\Psi}, \partial_y \overline{\Psi})$, Eq. (5) becomes

$$J(\Psi_{\text{res}}, \overline{b}) = \frac{\partial B}{\partial z} - \frac{\partial}{\partial y}[(1-\mu)\overline{\upsilon'b'}], \quad (6)$$

where $J(a, b) = \partial_y a \partial_z b - \partial_z a \partial_y b$; $\Psi_{\text{res}} = \overline{\Psi} + \Psi^*$ is the net or residual overturning circulation; the function $\mu = (\overline{w'b'}/\overline{\upsilon'b'})s_\rho^{-1}$ controls the magnitude of the diapycnal buoyancy flux due to the eddies and is often assumed to pass from 1 to 0 as z passes from the interior to the surface (e.g., Treguier et al. 1997). Thus, Eq. (6) implies that, in order for the interior residual circulation to follow mean isopycnals, that is,

$$J(\Psi_{\text{res}}, \overline{b}) \to 0, \quad (7)$$

the eddy buoyancy flux should be purely along mean isopycnals ($\mu = 1$) and, moreover, the small-scale mixing must be weak ($\partial_z B \to 0$).

We will return to this discussion in section 4 when analyzing the numerical model solutions. As we shall see, at eddy-permitting resolution the model vertical diffusivity does not have to be vanishingly small in order for the interior flow of deep water to be near adiabatic; hence, most of the deep-water upwelling occurs along isopycnals in the Southern Ocean. For now we note that (7) can hold when, for example, both the Eulerian mean and the eddy-induced flows have cross-isopycnal components that cancel each other, that is, $J(\overline{\Psi}, \overline{b}) = -J(\Psi^*, \overline{b}) \neq 0$, or when both the Eulerian mean and the eddy-induced flows tend to follow mean isopycnals, that is, $J(\overline{\Psi}, \overline{b}) \to 0$ and $J(\Psi^*, \overline{b}) \to 0$.

We will be employing four versions of the same numerical model that have different horizontal resolution (see next section). At the finest resolution considered, 0.2° (latitude) × 0.4° (longitude), the eddies can be said to be ''marginally permitted,'' whereas they become increasingly more ''parameterized'' with resolution decreasing to 0.3° × 0.6°, 0.6° × 1.2°, and 1.8° × 3.6°. The scheme that we employ to parameterize the effects of the unresolved mesoscale eddies is GM90. It assumes that, in the interior, the eddy buoyancy flux is along mean buoyancy surfaces (i.e., the eddies are ''adiabatic,'' which may not always hold—see appendix A). In the 2D case this can be expressed as follows:

$$\overline{\upsilon'b'}\partial_y \overline{b} + \overline{w'b'}\partial_z \overline{b} = 0. \quad (8)$$

Thus, in accordance with the above discussion, there should arise additional advective terms due to Ψ^* in the buoyancy budget. The eddy-induced streamfunction can be related to the resolved quantities such as the mean slope of isopycnals by adopting a simple closure for the eddy buoyancy flux (e.g., Gent et al. 1995), such that $\overline{\upsilon'b'} = -K\partial_y \overline{b}$. Then, using Eq. (8), the eddy-induced streamfunction in (4) is given by

$$\Psi^* = K s_\rho. \quad (9)$$

It then follows, particularly if one assumes that the eddy transfer coefficient K is constant, that for the parameterized eddy-induced flows to follow mean isopycnals [i.e., $J(\Psi^*, \overline{b}) \to 0$] the slope of isopycnals should do the same [i.e., $J(s_\rho, \overline{b}) \to 0$]. Clearly, the latter constraint would be difficult to maintain everywhere, so in general, particularly in the Southern Ocean, it is expected that $J(\Psi^*, \overline{b}) \neq 0$. We will return to this discussion in section 4. For now we note that in the numerical model we set K to a constant value that decreases with increasing model resolution (see also the next section). It should also be noted that the model we employ uses the equations for potential temperature and salinity, rather than for buoyancy, so there are additional terms representing mixing of temperature and salinity on isopycnal surfaces (diffusion of buoyancy on isopycnals is zero by definition).

We shall also be considering the role of the surface buoyancy input in setting the rate of diabatic transport in the uppermost ocean. Assuming that the corresponding diabatic–mixed layer (of thickness h_m) is vertically homogeneous and $B_{z=-h_m} = 0$ (see Marshall and

Radko 2003, 2006), integration of Eq. (5) across this layer gives

$$\Psi_{\text{res}|z=-h_m}\frac{\partial b_o}{\partial y} = B_o - (1-\mu)\int_{-h_m}^{0}\frac{\partial}{\partial y}\overline{v'b'}\,dz, \qquad (10)$$

where b_o and B_o are, respectively, the surface buoyancy and surface buoyancy flux. Following Speer et al. (2000a,b), we will try to diagnose the residual meridional transport in the upper Southern Ocean using B_o and will illustrate that the diabatic eddy fluxes cannot always be neglected (i.e., in general, $\mu \neq 1$).

We shall be analyzing not only the overturning circulation corresponding to the control model simulations, but also the changes in the Southern Ocean overturning, including those due to the projected strengthening of the local winds. At the latitudes of Drake Passage, the mean meridional geostrophic transport is zero above topography. It is therefore expected that the strength of the Eulerian mean overturning is largely given by the magnitude of meridional Ekman transport, $\overline{\Psi} = -\overline{\tau}/\rho f$, particularly when the averaging is taken along mean streamlines. If, in addition, the eddy-induced transport is parameterized according to Eq. (9), the residual overturning should be expected to scale as follows:

$$\Psi_{\text{res}} = -\frac{\overline{\tau}}{\rho f} + Ks_\rho, \qquad (11)$$

where f is the planetary vorticity (negative in Southern Hemisphere); $\overline{\tau}$ is the zonally averaged wind stress.

Hence, if the wind stress were to increase, the residual overturning would also tend to intensify, unless the eddy-induced transport (parameterized or permitted) compensates for such an intensification. At steady state, as follows from Eq. (10), a change in the residual flux within the mixed layer should be expected to be in balance with surface buoyancy flux and also with diapycnal eddy mixing. Further discussion of this important subject is given in section 5.

3. Numerical model

a. The University of Victoria Earth System Climate Model

This study uses version 2.7 of the intermediate complexity University of Victoria Earth System Climate Model (UVic ESCM). It couples a 3D ocean general circulation model, a 2D atmospheric model, a thermodynamic/dynamic sea ice model, and a simple land surface model and is described in detail in Weaver et al. (2001). The UVic ESCM has a global domain and model components share the same horizontal grid resolution.

The ocean component is version 2.2 of the Geophysical Fluid Dynamics Laboratory (GFDL) Modular Ocean Model (Pacanowski 1995). It has 19 vertical levels that increase parabolically in thickness from 50 m at the surface to 518 m at the deepest level. The vertical diffusivity ranges from 3.0×10^{-5} m^2 s^{-1} near the surface to 1.3×10^{-4} m^2 s^{-1} at depth according to the scheme of Bryan and Lewis (1979). Convective mixing is parameterized by an explicit full convection scheme described by Pacanowski (1995). Mixing of tracers associated with mesoscale eddies is parameterized according to GM90. The model employs the Boussinesq approximation. The barotropic momentum equations are solved by the implicit free-surface formulation of Dukowicz and Smith (1994). In low-stratification regions the GM90 slopes and tracer fluxes are tapered according to the scheme of Gerdes et al. (1991). Surface freshwater fluxes are converted to fluxes of salt with a constant salt-to-freshwater mass ratio of 3.49×10^{-2}.

The sea ice model incorporates energy-conserving ice–snow thermodynamics (Hibler 1979) and an elastic–viscous–plastic rheology (Hunke and Dukowicz 1997). The model predicts thickness and areal fraction of ice and snow, and surface temperature.

The UVic ESCM employs a vertically integrated energy–moisture balance atmospheric model for computational efficiency. Precipitation occurs when the relative humidity exceeds 90%, and on land soil moisture is treated by a simple bucket model described in Matthews et al. (2003). The UVic ESCM is forced from startup by insolation and surface winds. In the control simulations, winds are prescribed from the long-term monthly mean climatology of the National Centers for Environmental Prediction–National Center for Atmospheric Research (NCEP–NCAR) 50-Year Reanalysis (NCEP50; Kistler et al. 2001) and interpolated to match model resolutions.

b. Experimental design

Models with horizontal resolutions of $0.6° \times 1.2°$, $0.3° \times 0.6°$, and $0.2° \times 0.4°$ are initiated from the interpolated 3000-yr equilibrium state of a $1.8° \times 3.6°$ model. They are equilibrated under preindustrial (year 1900) orbital, atmospheric, and land surface conditions. Table 1 lists the values of the primary parameters modified in each model as well as their integration periods. Following the resolution criterion of Bryan et al. (1975), the horizontal mixing coefficient for momentum is reduced by roughly the factor increase in resolution (isopycnal tracer mixing coefficients were similarly reduced). Using this criterion, in our baseline model with the highest resolution ($0.2° \times 0.4°$) the Laplacian viscosity coefficient is set to a relatively large value of 1.5×10^4 m^2 s^{-1}

TABLE 1. Horizontal resolution parameters and integration periods of simulations. Here A_M, A_{ISO}, and A_{ITH} are the horizontal, isopycnal, and isopycnal thickness diffusion coefficients, respectively. The three highest-resolution models were initiated from the 3000-yr equilibrium state of the 1.8° × 3.6° model. All models are run on an upgraded NEC-SX6 supercomputer.

Horizontal resolution	1.8° × 3.6°	0.6° × 1.2°	0.3° × 0.6°	0.2° × 0.4°
A_M ($\times 10^4$ m^2 s^{-1})	20	7	3	1.5
A_{ISO} and A_{ITH} ($\times 10^2$ m^2 s^{-1})	4	1.5	1	0.75
Control integration length (yr)	3000	450	100	50
Forcing integration period (yr)	1900–2100	1900–2100	1900–2100	1900–2050
Model speed (yr day^{-1})	300	20	1.25	0.5

(Table 1). To make the dissipation more scale selective, one possibility is to employ the biharmonic form for lateral viscosity. However, this would require introducing different parameterizations for the different model resolutions—something we try to avoid in this intercomparison study. On the other hand, we would like to make a link with existing eddy-permitting models of the same or comparable resolution, such as the Fine Resolution Antarctic Model (FRAM). The FRAM is a primitive equation numerical model of the Southern Ocean (between 24° and 79°S) that has a horizontal resolution of 0.25° × 0.5°. It was started with a Laplacian viscosity of 0.2×10^3 m^2 s^{-1} and subsequently switched to biharmonic viscosity (Webb et al. 1991). Therefore, in addition to our baseline experiments listed in Table 1, we also discuss two experiments with the 0.2° × 0.4° model wherein the Laplacian viscosity coefficient was decreased to 10^3 m^2 s^{-1} and to 0.2×10^3 m^2 s^{-1}. These were run for only 5 yr, starting from the final control state (year 50) of the 0.2° × 0.4° baseline model run. The decrease of the viscosity coefficient results in an increase of eddy kinetic energy (EKE). In particular, averaged around 55°S, the near-surface EKE increases from 27 cm^2 s^{-2} in our baseline 0.2° × 0.4° model to 93 cm^2 s^{-2} when the horizontal viscosity is decreased to that of FRAM (zonally averaged EKE at 55°S is estimated from satellite altimetry to be 314 cm^2 s^{-2}; C. Wunsch 2008, personal communication). The filaments and plumes that characterize the Agulhas retroflection region of the baseline 0.2° × 0.4° model are found to generate more realistic warm core eddies in the reduced viscosity runs. It should, however, be noted that at this resolution such a reduction of the viscosity coefficient is expected to violate the Bryan et al. (1975) stability criterion, so that these additional runs are given only a brief discussion. On the other hand, the applicability of the Bryan et al. (1975) linear criterion to coupled model solutions based on primitive equations is not quite clear (e.g., Jochum et al. 2008).

While the horizontal resolution of each model component (ocean, land, atmosphere, and sea ice) is increased, only the ocean employs resolution-dependent surface data. Bathymetry was created for the three higher-resolution models by averaging the National Geophysical Data Center 5 arc minute gridded relief dataset (available online at http://www.ngdc.noaa.gov/mgg/fliers/93mgg01.html). The number of landmasses and the shape of coastlines were held fixed as resolution increased by placing a minimum 125 m (ocean level 2) depth constraint on new bathymetry features. All models have 19 vertical ocean levels and the same vertical ocean mixing coefficients. The vertical resolution is lower than in the FRAM, but is comparable to that employed in some global eddy-permitting ocean models (e.g., Semtner and Chervin 1988). A coarse vertical resolution was the computational sacrifice required to evaluate the overturning circulation in century rather than decade-long eddy-permitting simulations. Aside from the eddy-permitting simulation based on the global climate model developed at the Hadley Centre for Climate Prediction and Research, which is configured to have a resolution of 1/3° in its oceanic component (Roberts et al. 2004), presented herein are to our knowledge the longest integrated eddy-permitting global climate simulations currently available.

The integration times of the two highest-resolution models are still not sufficient to remove all long-timescale ocean transients induced upon switching resolution. Time step interval data from these models show weak trends in global ocean potential temperature and salinity of roughly +0.03 K century^{-1} and +0.0040 psu century^{-1}, respectively, after switching resolution. The range of global mean ocean potential temperature and salinity among the models is 3.35–3.60 K and 34.79–34.80 psu, respectively.

Models are forced from their control state with annually varying CO_2 concentrations and monthly surface wind anomalies. Computational constraints limit the forcing period of the 0.2° × 0.4° simulation to 150 yr (1900–2050); the three coarser-resolution models are integrated to 2100. The CO_2 concentration follows observations (295–365 ppm) over the first 100 yr and then increases to 830 ppm by 2100 following the Intergovernmental Panel on Climate Change (IPCC) Special Report

on Emissions Scenarios (SRES)-A2 scenario. Surface wind anomalies were assembled from a series of simulations performed by 10 different global climate models (forced by the same historical and SRES-A2 emissions trajectory) in support of the IPCC Fourth Assessment Report. Model-mean wind anomalies relative to 1900 were computed, temporally smoothed, corrected for a small equatorward bias (Fyfe et al. 2007), and then added to the NCEP50 climatology in the Southern Hemisphere only. The maximum zonal wind stress in the Southern Hemisphere increases by about 25% and shifts poleward by roughly 3.5° by the end of the twenty-first century.

4. Control simulations

a. Overturning circulation

In the oceanic interior where diabatic processes are weak, the circulation is expected to follow isopycnal surfaces. The position of these surfaces can significantly deviate from the surfaces of equal depth or pressure. Therefore, using potential density as the vertical coordinate, rather than the more traditionally used depth or pressure, can result in some major differences in the way the MOC is displayed. This was first illustrated by Döös and Webb (1994) and also by McIntosh and McDougall (1996) using a fine-resolution model of the Southern Ocean. It was shown, in particular, that the so-called Deacon cell, which normally appears when MOC is plotted as a function of depth, results from branches of equatorward and poleward flow occurring at the same densities but slightly different depths. The cell is characterized by an apparent sinking of surface waters to depths of 1000–3000 m between 40° and 50°S, creating an impression of mass flux across density surfaces. Döös and Webb (1994) demonstrate that Deacon cell is much reduced if instead of depth one uses potential density as the vertical coordinate.

Herein the meridional circulation is evaluated in density coordinates by first binning ocean model data onto 51 potential density levels with the difference between successive levels linearly decreasing from 0.3 to 0.085 kg m^{-3} as density increases. The choice of a reference density coordinate is known to affect the appearance of the overturning circulation (Hirst and McDougall 1998; Döös and Webb 1994). We evaluate the resolution dependence of the overturning circulation with a potential density coordinate referenced to 3000-m depth (σ_3) to clearly show intermediate depth waters.

Following Döös and Webb (1994), Döös et al. (2008), and K. Döös et al. (2008, unpublished manuscript), the streamfunction as a function of density is calculated as follows:

$$\Psi_{\rm res}(y,\sigma_3) = \frac{1}{t_1 - t_0}\int_{t_0}^{t_1}\oint\int_{-H(x,y)}^{z(x,y,\sigma_3,t)} v(x,y,z,t)\,dz\,dx\,dt, \tag{12}$$

where $v(x, y, z, t)$ is the meridional velocity binned into the (varying in time and space) σ_3 surfaces, $z(x, y, \sigma_3, t)$. This calculation is compatible with mass conservation in the model in that the overturning streamfunction integrated from the bottom goes to relatively small values at the surface [it is expected that because of the implicit free-surface formulation employed in the model, the streamfunction corresponding to instantaneous flows may not always be closed; since the emphasis here is on the deeper ocean, the integration in Eq. (12) is taken from the bottom].

Calculated this way, $\Psi_{\rm res}$ contains both the contribution from the time-mean circulation and that due to eddies (at eddy-permitting resolution), with the latter resulting from correlation between varying in time velocity and density. As in section 2, we will refer to it as to the ''residual'' streamfunction. To represent the evolution of v and σ_3, we use snapshots that are taken 5 days apart over a time integration interval of $t_1 - t_0$ equal to one year. As pointed out by McIntosh and Dougall (1996), and illustrated in K. Döös et al. (2008, unpublished manuscript), in a model where there is no strong interannual forcing, such as ours, using several years of snapshots instead of one year should not result in significant changes in this type of calculation. We tested an integration interval of three years for the 0.2° × 0.4° simulation and did not find a significant difference.

Figure 1 shows the residual MOC in the Southern Ocean calculated for the four different model resolutions. In each case, the meridional velocity represents the so-called effective transport, which is given by the sum of the resolved velocity and that due to the GM90 parameterization. However, the latter has a negligible influence on $\Psi_{\rm res}$ at 0.2° × 0.4°, whereas its influence increases with the decrease in the model resolution. Of particular interest is the clockwise circulation associated with the southward-flowing Circumpolar Deep Water (CDW), its upwelling into the mixed layer, conversion into lighter Antarctic Intermediate Water (AAIW), and then the AAIW subduction from the mixed layer into the oceanic interior. It can be seen from the figure that this circulation cell depends qualitatively on the model resolution. Essentially, in the two coarsest-resolution model versions there are significant [≈10 Sv (1 Sv ≡

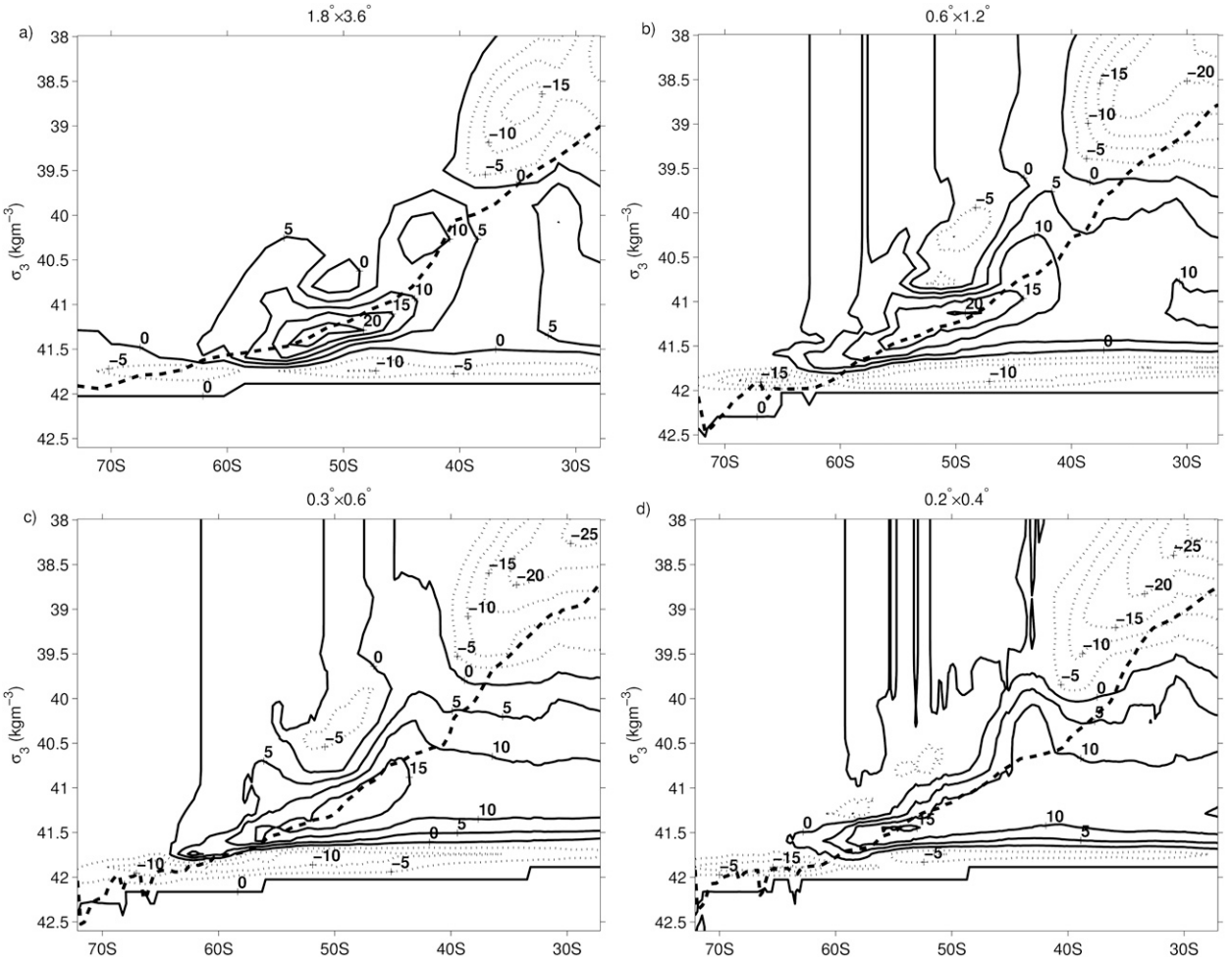

FIG. 1. Southern Ocean Ψ_{res} in the control state of the simulations. Horizontal resolutions of (a) 1.8° × 3.6°, (b) 0.6° × 1.2°, (c) 0.3° × 0.6°, and (d) 0.2° × 0.4°. Streamlines (5-Sv contour intervals) are plotted as a function of potential density referenced to 3000-m depth (σ_3). Solid lines (positive values) and dotted lines (negative values) indicate clockwise and counterclockwise flow, respectively. The thick dashed line is a proxy for the maximum density of the mixed layer.

10^6 m^3 s^{-1})] diapycnal fluxes between about 40° and 50°S (Figs. 1a,b). These diapycnal fluxes allow for a formation of closed Deacon cells despite our use of potential density as the vertical coordinate, rather than depth. Qualitatively similar but weaker diapycnal fluxes (≈5 Sv) forming a closed Deacon cell in density space have been reported by Drijfhout (2005) (bottom panel in his Fig. 10) in an eddy-permitting model.

At resolutions of 1.8° × 3.6° and 0.6° × 1.2°, the zonal mean clockwise Southern Ocean overturning is essentially decoupled from, or only weakly coupled to, the rest of the World Ocean (Figs. 1a,b; cf. Figs. 6b,d in Gnanadesikan et al. 2006). In contrast, as the model resolution increases, the Deacon cell becomes much weaker, barely appearing (as a closed cell) in the model version with the highest resolution employed (Fig. 1d), that is, at 0.2° × 0.4°. At this resolution, the CDW upwells adiabatically into the mixed layer (around 60°S and along about $\sigma_3 = 41.7$) and, after being transformed into AAIW, it outflows from the mixed layer (around 40°S and between about $\sigma_3 = 39.5$ and 40.5) and flows northward also near adiabatically. Hence, as the model resolution increases, the zonal mean circulation associated with the upwelling of CDW and outflow of AAIW tends to follow isopycnals (Figs. 1c,d), thereby more effectively connecting the Southern Ocean to the rest of the World Ocean.

The weaker coupling between the Southern Ocean MOC and the rest of the ocean seen in the coarse-resolution model versions implies that light-to-dense water transformation in the North Atlantic, and the associated formation of North Atlantic Deep Water (NADW), is mostly compensated for by dense-to-light water conversion at low latitudes (Fig. 2a). Hirst and

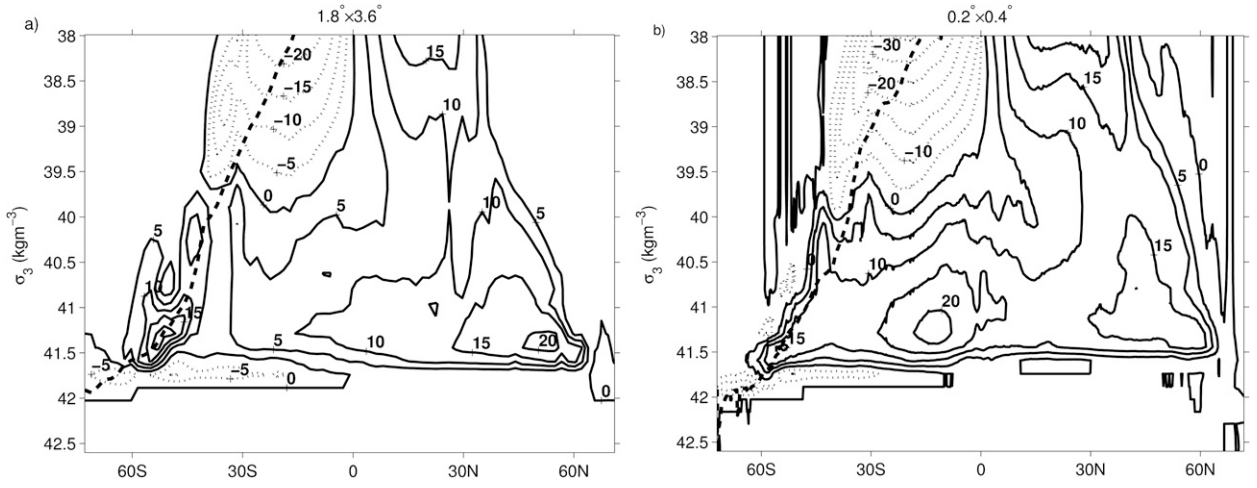

FIG. 2. The Ψ_{res} for the global ocean in the control state at (a) 1.8° × 3.6° and (b) 0.2° × 0.4°. Plotted in the same manner as Fig. 1.

McDougall (1998), using a 1.6° × 2.8° model, also simulate such an extreme situation for their MOC in latitude–density space (see their Figs. 4 and 5). Similar to our model, the Hirst and McDougall (1998) model uses the Bryan and Lewis (1979) profile to represent vertical diffusivity K_v with values at the base of the pycnocline of about 0.4×10^{-4} m^2 s^{-1}. Using the advective diffusive scaling (i.e., $Aw = AK_v/h$, with A and h being, respectively, the area of low-latitude ocean and mean depth of pycnocline), such K_v values can account for the deep water upwelling through the low-latitude ocean of the order of 10 Sv (with $A = 2.5 \times 10^{14}$ m^2, $h = 10^3$ m and $K_v = 0.4 \times 10^{-4}$ m^2 s^{-1}, $Aw = 10$ Sv). In contrast, the MOC simulated by the high-resolution model versions has the tendency for a more adiabatic circulation of NADW in the interior (Fig. 2b), so that about ⅔ of NADW forming in the northern North Atlantic (10 Sv out of 15 Sv) upwells in the Southern Ocean. (Note that the closed overturning cell centered near 15°S and $\sigma_3 = 41.3$ in Fig. 2b is predominately a feature of the Indian Ocean circulation.) Such a tendency for a more adiabatic circulation in the interior is formally expressed by Eq. (7). However, when deriving Eq. (7) we assumed that the small-scale mixing in the interior is weak, whereas, in the high-resolution models, the tendency for a near-adiabatic residual circulation in the interior is established despite our use of the same profile for vertical diffusivity (and the same criteria for convective mixing) as in the coarse-resolution models. This means that, as the resolution increases, the overturning circulation becomes less sensitive to the representation of some subgrid-scale processes. As a result, despite our use of relatively large values for K_v in the pycnocline, the NADW tends to upwell less through the low-latitude oceans and more in the Southern Ocean. This may not always be easy to deduce from simple, scaling-based models of the global ocean overturning circulation, such as, for example, that of Gnanadesikan (1999).

To separate the contributions to Ψ_{res} arising because of the mean and eddy-induced components of the circulation, we introduce the following streamfunction (e.g., Döös et al. 2008; K. Döös et al. 2008, unpublished manuscript):

$$\overline{\Psi}(y,\sigma_3) = \oint \int_{-H(x,y)}^{\overline{z}(x,y,\sigma_3)} \overline{v}(x,y,\overline{z})\, d\overline{z}\, dx, \qquad (13)$$

where time averaging is performed first, so that $\overline{v}(x,y,\overline{z})$ is the averaged in time meridional velocity binned into the (varying only in space) σ_3 surfaces, $\overline{z}(x,y,\sigma_3)$. Then, the eddy contribution to the residual streamfunction can be estimated as follows (e.g., Döös et al. 2008a; K. Döös et al. 2008, unpublished manuscript):

$$\Psi^* = \Psi_{res} - \overline{\Psi}. \qquad (14)$$

Calculated this way, the eddy-induced streamfunction in the 0.2° × 0.4° baseline model is shown in Fig. 3a. For comparison, shown in Figs. 3b,c are the eddy-induced streamfunctions corresponding to the 0.2° × 0.4° model versions with reduced viscosity, as described in the experimental design section. The eddy-induced flow has a strong diapycnal component, with much of it confined to the mixed layer. With decreasing viscosity, the rate of eddy-induced overturning increases and it tends to penetrate to denser water classes. For comparison, Fig. 3d presents the overturning in the 1.8° × 3.6° model due to the GM90 eddy-induced velocity. The streamfunction induced by the parameterized eddies resembles those induced by the permitted eddies in that its

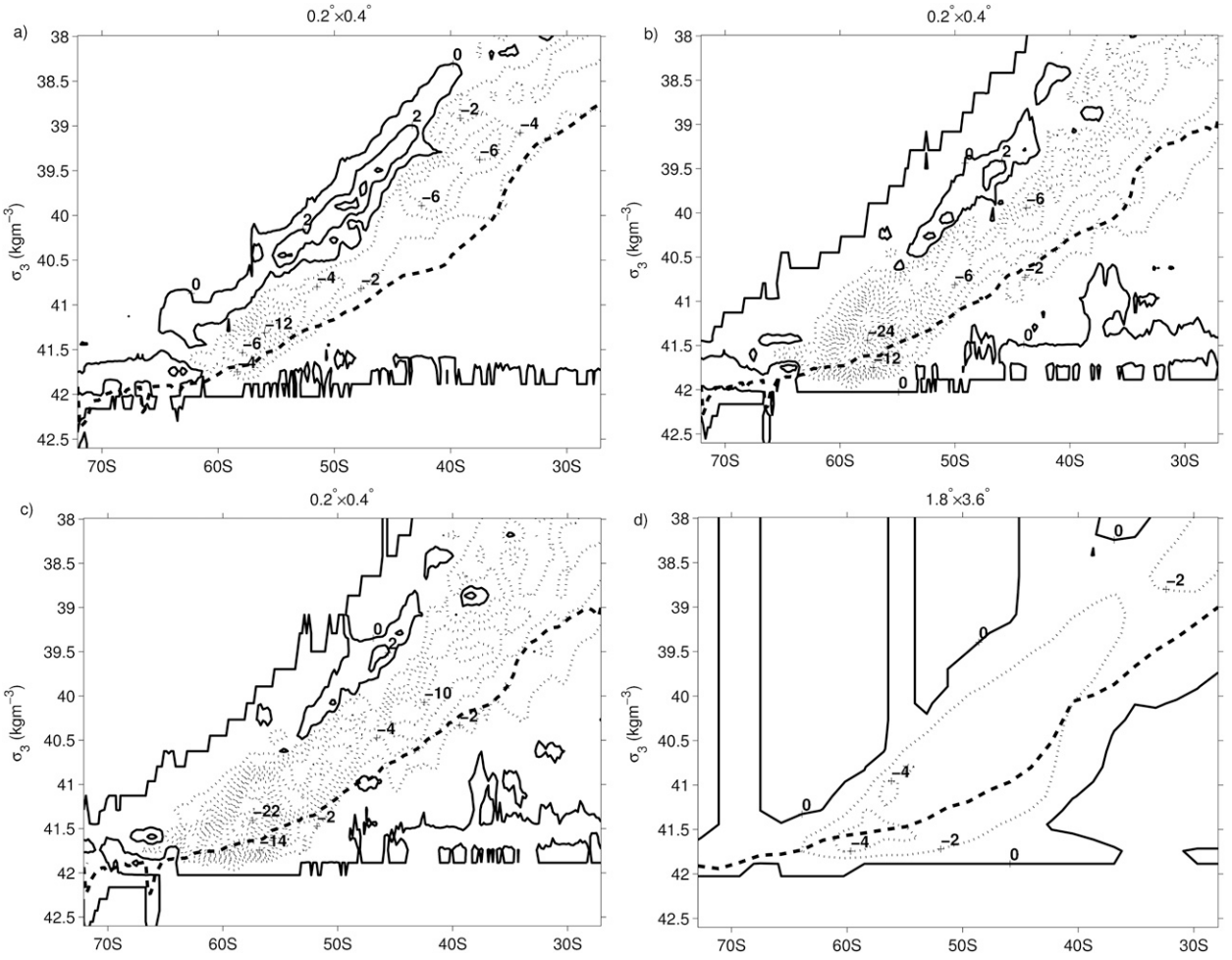

FIG. 3. (a) Resolved Ψ^* for the Southern Ocean in the control state of the baseline $0.2° \times 0.4°$ model ($A_M = 1.5 \times 10^4$ m^2 s^{-1}). (b),(c) Resolved Ψ^* at $0.2° \times 0.4°$ with A_M reduced to 10^3 m^2 s^{-1} and 2×10^2 m^2 s^{-1}, respectively. (d) The GM90 Ψ^* at $1.8° \times 3.6°$. Plotted in the same manner as Fig. 1, except with 2-Sv contour intervals.

maximum is positioned between 50° and 60°S, although it is weaker (its strength depends on the value imposed for the coefficient of layer thickness diffusivity in the GM90 mixing scheme). In addition, the permitted eddies thus defined (i.e., as deviations from the annual mean state) can induce strong recirculating flows within the mixed layer (Figs. 3a–c), which are absent or much weaker than when the eddies are parameterized (Fig. 3d). Part of the reason for this is that, as noted, the ''eddies'' defined as deviations from a mean state obtained by averaging over one or several years are expected to include seasonal variability.

The impact of the seasonal variability can be reduced by noting that a more appropriate averaging operator in Eq. (13) would be a low-pass operator, which would allow the mean variables to evolve with time (McDougall and McIntosh 1996). Replacing the long-term averaging in Eq. (13) by an averaging for each of the four seasons, the eddy cells in the mixed layer are strongly suppressed and the streamfunctions induced by the permitted eddies (Figs. 4a–c) more closely resemble those induced by the parameterized eddies (Fig. 4d). Both the permitted and the parameterized eddies induce closed overturning cells extending below the mixed layer in the Southern Ocean, between about 50° and 60°S. This is consistent with previous studies (e.g., see Fig. 6b in Hirst and McDougall 1998; Fig. 4c in Speer et al. 2000a; Fig. 4 in Saenko et al. 2005; see also Gent et al. 1995) and is also in general agreement with a recent simulation based on an eddy-resolving ($^1/_{12}°$) model (Lee et al. 2007; see their Fig. 5b). Differences between the seasonally and annually averaged eddy-induced overturning circulations are predominately found within the mixed layer, precisely where the use of GM90 parameterization is most questionable, and where the net effect of GM90 on the overturning depends

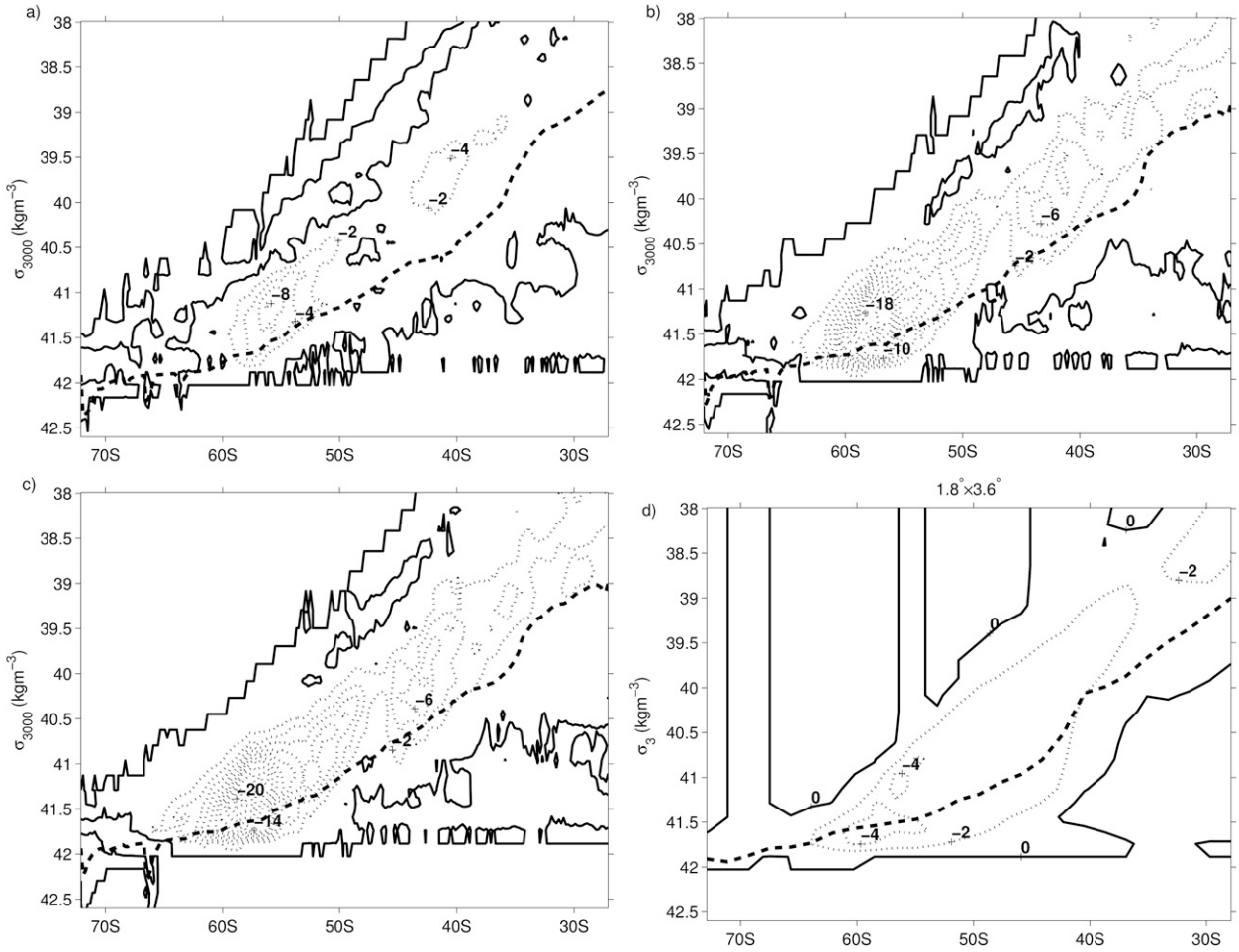

FIG. 4. (a) Resolved Southern Ocean Ψ^* (2-Sv contours) in the baseline $0.2° \times 0.4°$ model ($A_M = 1.5 \times 10^4$ m^2 s^{-1}) calculated with a seasonal time average operator. Same as in (a), but with A_M reduced to (b) 10^3 m^2 s^{-1} and (c) 2×10^2 m^2 s^{-1}, respectively. (d) The GM90 Ψ^* at $1.8° \times 3.6°$.

on isopycnal slope tapering schemes (see Danabasoglu et al. 2008).

b. Water mass transformation

Equation (10) suggests that if 1) the surface buoyancy flux dominates the diapycnal mixing within the mixed layer, 2) below the mixed layer the diapycnal mixing is weak, and 3) internal sources of buoyancy are negligible, then within the outcropping isopycnals the residual overturning circulation can be estimated using only the surface buoyancy flux. This idea was originally proposed by Walin (1982) for the circulation associated with surface heat flux and has been further elaborated in a number of more recent studies (e.g., Iudicone et al. 2008). Essentially, the net mass transport in the direction of increasing buoyancy within the mixed layer (i.e., a conversion from dense water to lighter water) would be favored by a buoyancy gain at the surface, whereas a conversion from light water to denser water would be favored by a buoyancy loss.

Some of the above assumptions may not always be easy to justify. For example, the diapycnal mixing in the near-surface ocean, such as that arising because of the diabatic component of mesoscale eddy buoyancy flux, may not be weak (e.g., Radko and Marshall 2004). In this regard, the question we would like to address here is how much of the cross-isopycnal volume transport in the Southern Ocean mixed layer, particularly within the density ranges of the CDW-to-AAIW conversion, can be attributed to the surface buoyancy flux.

The quantity that is estimated in practice is the so-called transformation rate from one buoyancy class to another (e.g., Speer et al. 2000a,b), given by

$$\mathcal{F}(b') = \int_{\text{year}} dt \iint_{\text{area}} -B_o \, dx \, dy \, \delta[b(x,y,t) - b'], \quad (15)$$

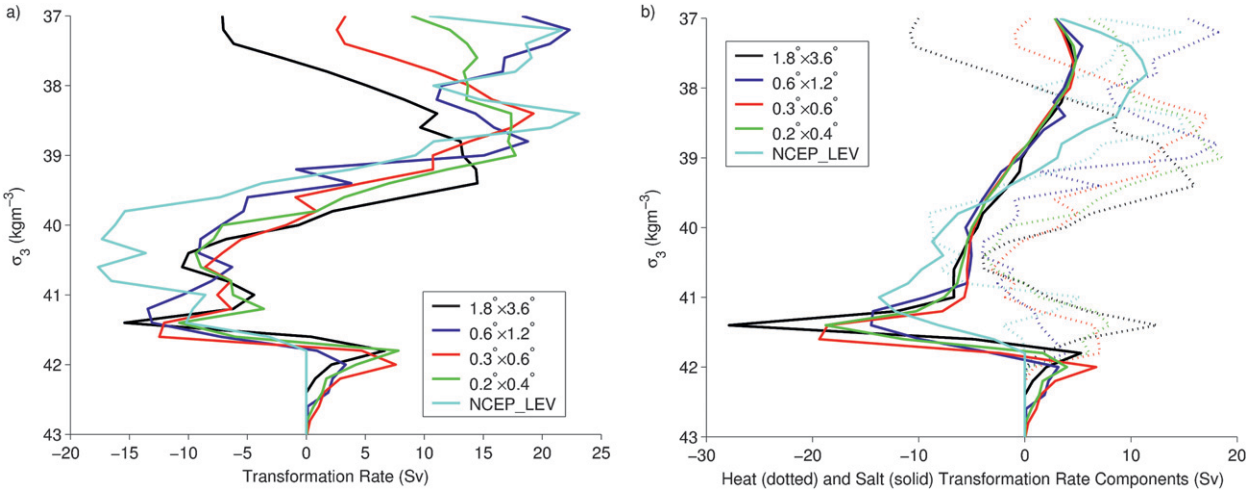

FIG. 5. Residual transformation rates ($\mathcal{F}$) of Southern Ocean water masses for each of the UVic ESCM simulations as well as a dataset composed of NCEP reanalysis surface fluxes and Levitus sea surface climatology. (a) The total transformation rates and (b) separated into surface heat (dotted lines) and salt (solid lines) flux components.

with the δ function permitting sampling of the surface buoyancy flux B_o only for surface water of buoyancy b. The surface buoyancy flux is given by

$$B_o = -\frac{g\alpha}{\rho_o C_w} H(x,y,t) + \frac{g\beta S_o}{\rho_o} W(x,y,t), \qquad (16)$$

where g is the gravitational constant; $\alpha = -\rho^{-1}(\partial\rho/\partial T)_{p,s}$; $\beta = \rho^{-1}(\partial\rho/\partial S)_{p,T}$; C_w is the specific heat of water; ρ_o and S_o are the reference density and salinity; and H and W are, respectively, the net heat and freshwater fluxes. The transformation rate estimated this way, once again, combines both the advective and diffusive components of the buoyancy transport (Garrett et al. 1995; Speer et al. 2000a,b; see also appendix B).

As the first step, we compare the model-derived transformation rates in the Southern Ocean with a transformation estimate based on observations. In the latter case, we use a dataset (hereafter referred to as NCEP_LEV) that comprises the NCEP50 reanalysis model surface fluxes (Kistler et al. 2001) and the Levitus sea surface climatology (Levitus et al. 1994; Levitus and Boyer 1994). The main focus is on the model version with the highest resolution where, as we have seen (Fig. 1d), the cross-isopycnal volume flux in the mixed layer can serve as a good proxy for the near-adiabatic interior circulation associated with the upwelling of CDW and subduction of AAIW. However, it is also of interest to compare the transformation rates for all four UVic ESCM simulations.

The UVic ESCM transformation rates have similar profiles in all four simulations and three principle density classes of transformation are identifiable (Fig. 5a). [Note that we use σ_3 in this and all other figures showing transformation rates, which is motivated by our desire to be able to directly compare $\mathcal{F}(\sigma_3)$ with the overturning circulation where we also use σ_3; only small differences are found in the shape of the transformation curves when using σ_0 instead of σ_3.] These density classes correspond to the surface waters of the three cells found in the MOC (Fig. 1). Surface water in the highest density class ($\sigma_3 > 41.7$), corresponding to polar cell waters, is gaining density in the UVic ESCM simulations. Separating $\mathcal{F}$ into haline and thermal components (Fig. 5b) demonstrates that the formation of Antarctic Bottom Water (AABW) is dominated by surface salt fluxes resulting from brine rejection during sea ice formation. Transformation in this density class for the NCEP_LEV dataset is zero because the reanalysis data do not explicitly include brine rejection and also because in the high latitudes the Levitus data are dominated by summertime observations. In all five datasets, both haline and thermal forcings play a role in transforming the surface water of the CDW–AAIW cell ($39.5 < \sigma_3 < 41.7$). In the UVic ESCM simulations the lightening of these subpolar cell surface waters by haline forcing dominates a weak density gain by heat loss in the $40.8 < \sigma_3 < 41.7$ density range, while both heat gain and salt loss are responsible for the lightening in the $39.5 < \sigma_3 < 41$ density range. Similar results are found for NCEP_LEV data with the exception of greater haline and thermal forcing between $39.8 < \sigma_3 < 41.3$, which increases the net transformation rate over this density range relative to the UVic ESCM simulations. The gain in density of subtropical cell water ($\sigma_3 < 39.5$) is primarily

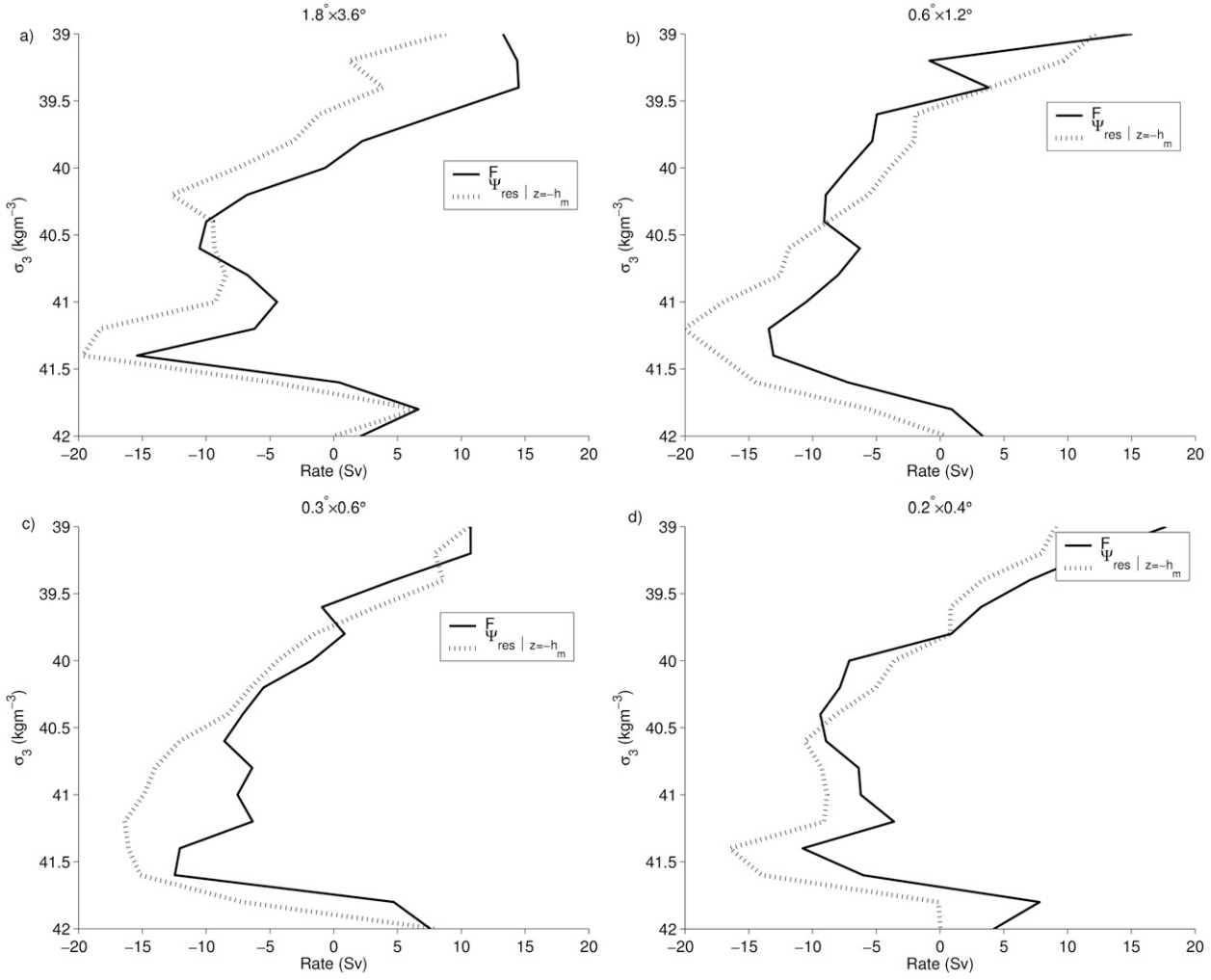

FIG. 6. Residual transformation rate ($\mathcal{F}$) of CDW/AAIW water masses along with the residual transport through the base of the mixed layer ($\Psi_{\mathrm{res}|z=-h_m}$) in the control simulations. Note that in these plots negative $\Psi_{\mathrm{res}|z=-h_m}$ values represent northward transport.

the result of surface heat loss and salt gain in all five datasets.

As noted, to the extent that the surface buoyancy flux dominates the eddy diapycnal mixing within the mixed layer, the residual cross-isopycnal volume flux within the layer, $\Psi_{\mathrm{res}|z=-h_m}$, is expected to be compatible with $\mathcal{F}$. Qualitatively, within the density classes of the CDW-to-AAIW conversion ($39.5 < \sigma_3 < 41.7$), which is of major interest here, all models show such a compatibility (Fig. 6). The focus, however, is on the $0.2° \times 0.4°$ model, where eddies are permitted and where the diapycnal flux within the mixed layer is a good proxy for the near-adiabatic circulation of CDW–NADW and AAIW in the interior. From Fig. 6d, it can be seen that, for this density range, except perhaps at its upper limit, the volume transport within the mixed layer simulated by the $0.2° \times 0.4°$ model is well captured by the corresponding transformation rate. For the densest waters within this range (around $\sigma_3 = 41.2$), only about 50% of the cross-isopycnal volume transport is accounted for by the surface buoyancy flux (Fig. 6d). This suggests that the buoyancy flux arising because of the diabatic component of the (permitted) mesoscale eddies can, for some density classes, be of the same order as the surface buoyancy flux and, hence, cannot be neglected. Thus, it may not always be possible to infer $\Psi_{\mathrm{res}|z=-h_m}$ from $\mathcal{F}$, consistent with Treguier et al. (2007). However, for some density classes, $\mathcal{F}$ can be a good proxy for $\Psi_{\mathrm{res}|z=-h_m}$ (Fig. 6d) and, hence, for the corresponding near-adiabatic circulation in the interior.

Can this be useful? First, it takes time for the interior flows to come into equilibrium with the surface boundary conditions and, second, a change in the circulation could feed back on surface fluxes. Nonetheless, these

results suggest that, in some cases, it might be possible to infer the interior circulation from the surface buoyancy flux. Moreover, one may hope to diagnose changes in the circulation in response to a changing climate, which, at steady state, are expected to be largely compatible with changes in the surface buoyancy flux. However, such a compatibility, as we shall see next, may not always be insured at the transient stage of the circulation-flux adjustment.

5. Projected changes

In this section, we briefly consider projected twenty-first-century changes in the circulation associated with the upwelling of CDW and its conversion to AAIW. An expectation is that this conversion may increase for two reasons. First, the wind stress, which is imposed in the models to correspond to that projected for the twenty-first century (Fyfe et al. 2007), increases over the Southern Ocean, particularly its zonal component. Hence, the Eulerian mean overturning should also increase; this could, at least in part, be compensated by the eddy-induced return flow. Second, with the increasing concentration of greenhouse gases, the buoyancy gain in the subpolar oceans, including in the Southern Ocean, is expected to increase both because of the associated warming and enhanced precipitation. Again, this could be partly compensated by the diabatic eddy fluxes. Furthermore, as the concentration of greenhouse gases increases and the upper ocean warms up more than the deeper ocean, it is expected that the oceanic stratification will also generally increase. This has a potential to influence, for example, the low-latitude upwelling of deep water and the eddy-induced transport. Overall, how (and if) all these and other changes would translate into the changes in the overturning circulation is not easy to foresee.

The focus is on the circulation projected by the two model versions with higher resolution. Since running the 0.2° × 0.4° model is computationally quite expensive, it was only integrated to obtain the projection by the middle of the twenty-first century. We note, however, that the Southern Ocean wind stress is projected to become much stronger from 2050 to 2100 (Fyfe et al. 2007; Saenko 2007), so that a change in the overturning circulation by the middle of the twenty-first century may differ from that projected by the century end, although one would not expect qualitative differences.

According to the 0.3° × 0.6° model, the MOC corresponding to the density range of main interest here (roughly $39.5 < \sigma_3 < 41.7$) does not slow down (Fig. 7a). Rather, by the end of the twenty-first century it is projected to intensify (Fig. 7c). This intensification is not confined to the Southern Hemisphere; rather, on these time scales it is carried into the Northern Hemisphere (not shown). However, the amplitude of this cross-equatorial penetration of the overturning circulation anomaly from the south to the north may depend on the model's ability to capture the adjustment processes due to coastal and equatorial Kelvin waves. Further discussion of this important process is beyond our scope here (but see Johnson and Marshall 2004). The 0.2° × 0.4° model, which has been run only until the middle of the twenty-first century, also projects an intensification of the Southern Ocean MOC (Figs. 7b,d).

Further insight can be obtained by considering the projected changes in the transformation rates that, together with the corresponding mixed layer transports, are shown in Fig. 8. Since we deal with transient changes in the circulation, these should not be expected to be as compatible with the transformation rates as they are in the control simulations. Nevertheless, we have demonstrated that, for many density classes at steady state, the circulation implied by $\mathcal{F}$ is compatible with $\Psi_{\mathrm{res}|z=-h_m}$ (Fig. 6). Therefore, it seems reasonable to expect that, at near steady state, there would be a similar compatibility between $\mathcal{F}$ and $\Psi_{\mathrm{res}|z=-h_m}$ in the future.

According to the 0.3° × 0.6° model, both $\mathcal{F}$ and $\Psi_{\mathrm{res}|z=-h_m}$ increase by more than 10 Sv around $\sigma_3 = 40$ (Fig. 8c) by year 2100. Projected changes in $\mathcal{F}$ and $\Psi_{\mathrm{res}|z=-h_m}$ by the 0.2° × 0.4° model indicate a strong increase around $\sigma_3 = 41$ by year 2050 (Fig. 8d). Neither model shows a decrease in CDW-to-AAIW conversion, and both simulations show that much of the increase in $\Psi_{\mathrm{res}|z=-h_m}$ is due to the local recirculation (Figs. 7c,d), with only a fraction of it extending further north. However, given the tendency for a near-adiabatic circulation of deep water under the near-steady conditions (Fig. 1d), the projected local diabatic recirculation (Fig. 7b,d) should be expected to decrease on longer time scales, thereby increasing the positive overturning circulation anomaly penetrating to the Northern Hemisphere.

6. Discussion and conclusions

Climate models are extensively employed for studying the climate variability associated with changes in the ocean MOC. The bulk of the previous work has focused on the northern North Atlantic, where a conversion from light to dense waters and the associated formation of NADW can be sensitive to surface buoyancy input. However, the MOC is also expected to be influenced by dense-to-light water conversion processes, as occurs in the Southern Ocean—a region of strong mesoscale eddy

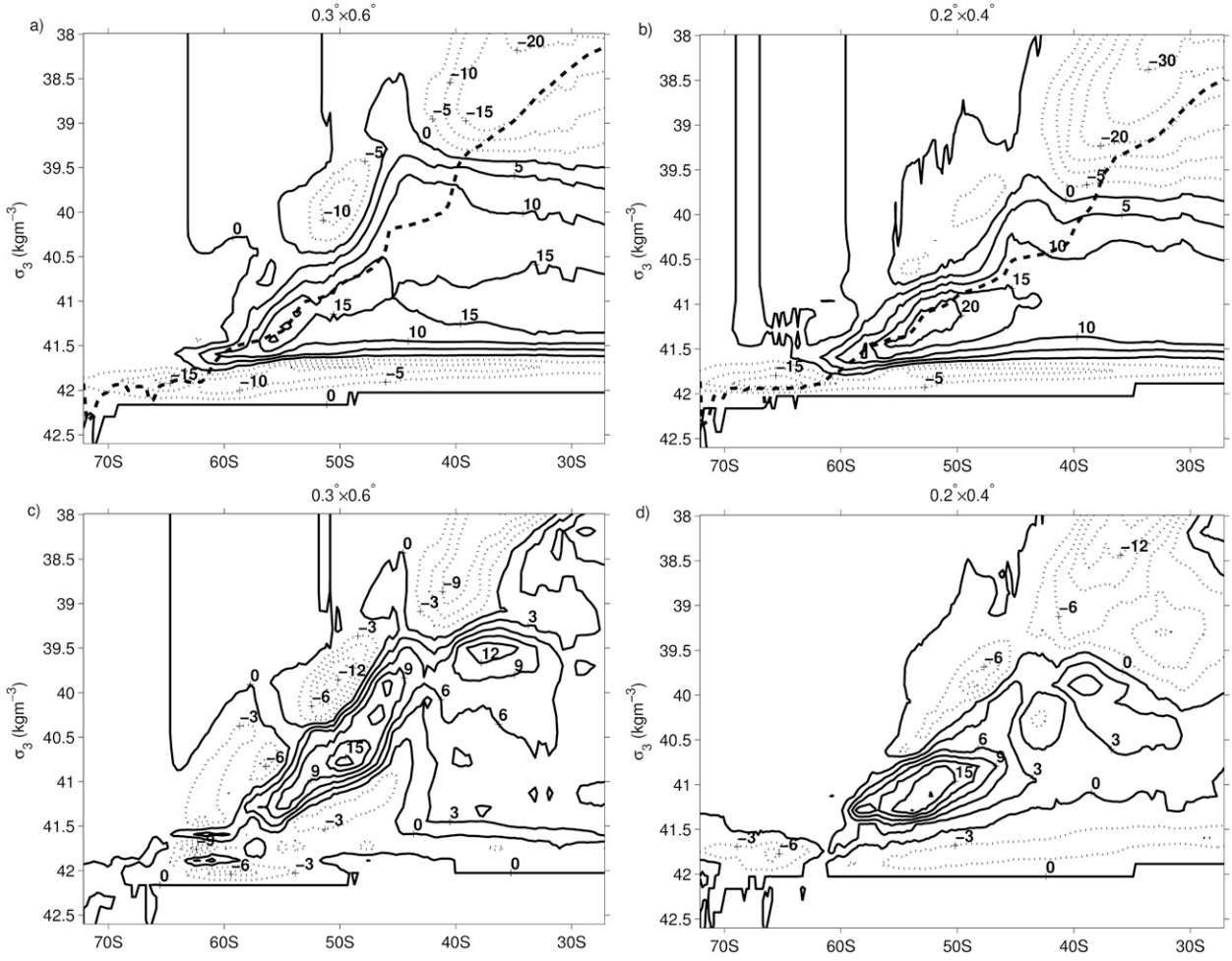

FIG. 7. (a) Year 2100 Ψ_{res} at 0.3° × 0.6° and (b) year 2050 at 0.2° × 0.4° (5-Sv contour intervals). (c),(d) The Ψ_{res} anomalies (3-Sv contour intervals) relative to the year 1900 control state.

activity. Whereas a great deal of the earlier work in this area has been based on coarse-resolution models with mesoscale processes being heavily parameterized, the Southern Ocean branch of the MOC and its response to changes in the climate could be quite sensitive to the representation of mesoscale effects in models.

Here, we have employed four versions of the same climate model with horizontal resolutions ranging from 1.8° × 3.6° to 0.2° × 0.4°. As the resolution increases and, in particular, as eddy effects become less parameterized, the deep water forming in the North Atlantic tends to upwell more in the Southern Ocean and less in the low-latitude oceans. At the highest resolution employed (0.2° × 0.4°), out of 15 Sv of diapycnal light-to-dense water conversion in the north (around 60°N and across isopycnals between $40.5 < \sigma_3 < 41.5$), about 10 Sv upwells in the Southern Ocean. In contrast, in the coarse-resolution model versions, most of the NADW upwells at low latitudes, so that the Southern Ocean becomes, on zonal mean, less coupled with the rest of the ocean. This is despite our use of the same profile for vertical diffusivity in all four model versions, with values that (potentially) allow for as much as 10 Sv of dense-to-light water transformation through the low-latitude pycnocline.

We find that, as the resolution increases, the interior residual circulation within the density range of CDW-to-AAIW conversion becomes more adiabatic. However, both the permitted eddies in the highest-resolution model versions and the eddies parameterized using the GM90 scheme induce closed overturning cells in the Southern Ocean, with maxima centered between 50° and 60°S. This is in agreement with a recent simulation based on an eddy-resolving (1/12°) model (Lee et al. 2007). We note, however, that the GM90 parameterization is based on the assumption of adiabatic eddy

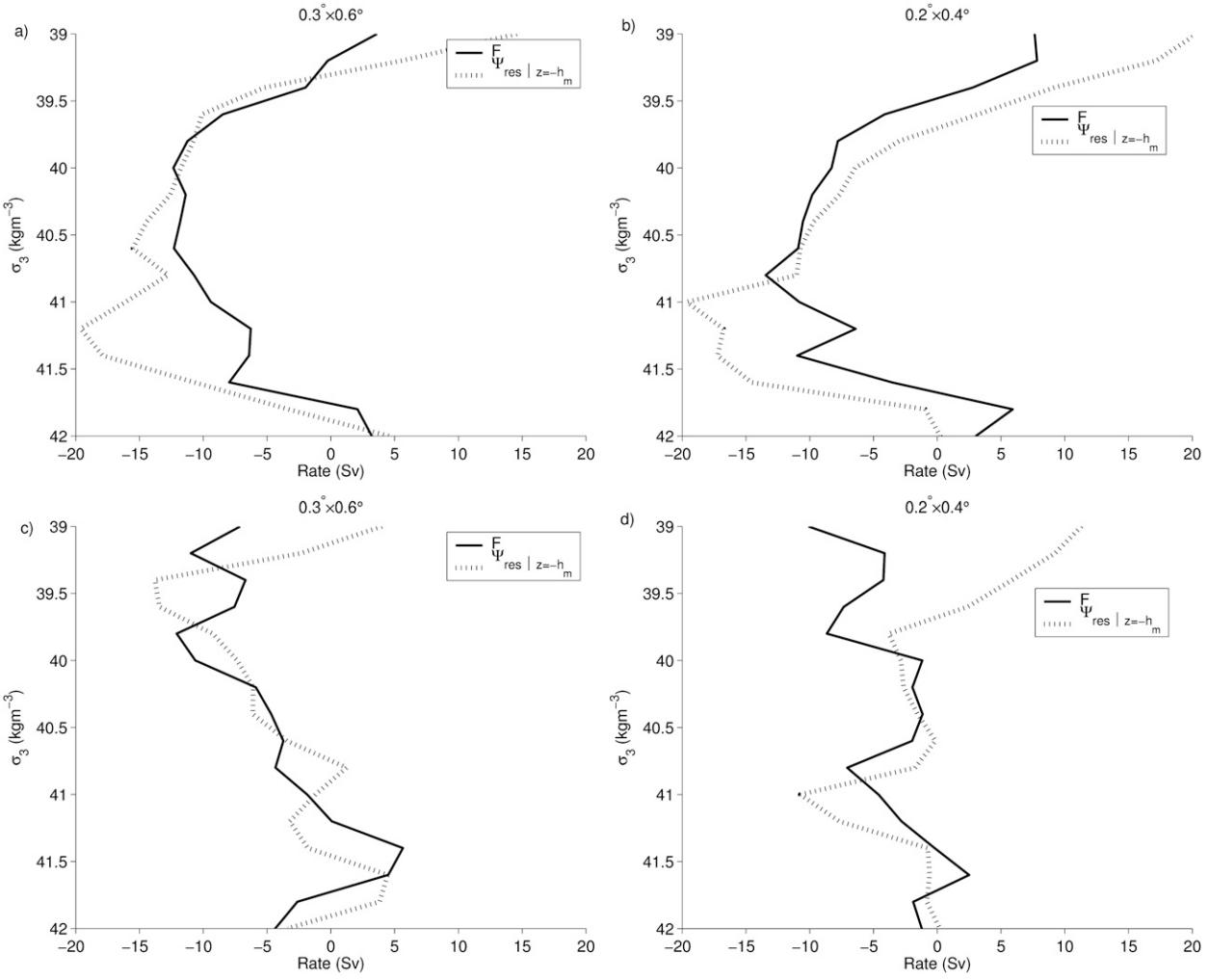

FIG. 8. The $\mathcal{F}$ and $\Psi_{\text{res}|z=-h_m}$ in year 2100 and 2050 at (a) 0.3° × 0.6° and (b) 0.2° × 0.4°. (c),(d) Anomalies relative to year 1900.

buoyancy fluxes, which, in general, does not hold (McDougall and McIntosh 1996; Treguier et al. 1997; see also appendix A), including in numerical simulations (Cerovečki et al. 2009). In addition, while the relation between surface buoyancy flux and meridional streamfunction in the Southern Ocean has been questioned by Treguier et al. (2007), we find that for many density classes the so-called transformation rate is a good proxy for the interior circulation, although in general the diapycnal eddy fluxes in the mixed layer cannot be neglected.

Finally, we use two model versions with higher resolution to project future changes in the MOC in response to changes in the climate induced by accumulation of greenhouse gases in the atmosphere. For the latter, we use the IPCC SRES scenario A2. Since the atmospheric component of the model is rather simple, the corresponding changes in the wind stress are imposed. These are derived from a set of climate change projections based on fully coupled models.

At least two factors are of major importance to the Southern Ocean MOC response. The first is related to the projected strengthening in the Southern Ocean zonal wind stress. This tends to intensify the Eulerian mean component of the overturning, which can be partly or totally offset by strengthening of the eddy-induced overturning. Second, the projected stronger buoyancy input at the surface in the subpolar oceans, while favoring a reduction of light-to-dense water transformation in the northern North Atlantic, favors an intensification of the reverse process in the Southern Ocean. The overall effect of these changes on the upper-ocean MOC in the warmer climate is difficult to foresee. However, based on these model results, it can be concluded that on a century-long time scale, the circulation associated with the CDW-to-AAIW conversion is more

likely to intensify, rather than to slow down, in general agreement with discussions presented in Toggweiler and Russell (2008) and Saenko (2007). This should be expected to eventually affect the rate of light-to-dense water conversion in the Northern Hemisphere and the associated flow of NADW in a warmer climate. In particular, increasing oceanic resolution from 1.25° to 1/3°, Roberts et al. (2004) found a less pronounced weakening of the meridional overturning and heat transport in the Atlantic in their climate model in response a 2% yr^{-1} increase in CO_2. More recently, Delworth and Zeng (2008) simulated an intensification of the Atlantic MOC in response to a change in the Southern Ocean wind stress similar to that imposed in our study but using the GFDL fully coupled model and keeping other forcings unchanged.

Taken together, our results demonstrate that the conversion of dense waters back to light waters is sensitive to the degree of parameterization of mesoscale eddies in models. In turn, horizontal resolution should be considered when evaluating the overturning circulation.

Acknowledgments. This research was supported by the NSERC/CFCAS CLIVAR program. Infrastructure support from CFI, NEC, BCKDF, and the University of Victoria is also acknowledged. Thank you to Chris Avis, Alvaro Montenegro, and Matthew England for their helpful comments.

APPENDIX A

Are Eddy Fluxes Directed along Mean Isopycnals?

Here we closely follow some of the discussion in McDougall and McIntosh (1996) and Treguier et al. (1997) to illustrate that, in general, the assumption that eddies are adiabatic, which is assumed in the GM90 parameterization, should not be expected to hold (see also McDougall and McIntosh 2001; McDougall et al. 2007). Consider the conservation equation for buoyancy,

$$b_t + \mathbf{U} \cdot \nabla b = Q, \tag{A1}$$

where $\mathbf{U}$ is the three-dimensional velocity vector and Q represents the unresolved small-scale mixing processes (internal sources of buoyancy may also be included). Applying a Reynolds decomposition to each variable (i.e., $\lambda = \overline{\lambda} + \lambda'$) and using the standard procedure (McDougall and McIntosh 1996), it is straightforward to derive the conservation equation for (half) the buoyancy variance, $\phi \equiv \frac{1}{2}(b')^2$:

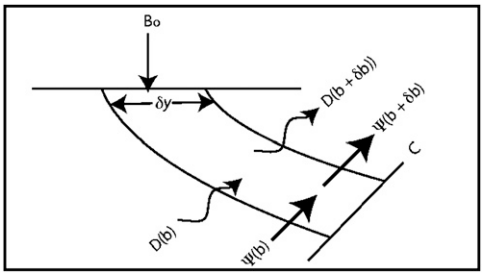

FIG. B1. Schematic of diapycnal transfer motion between two outcropping isopycnals bounded at depth by a control surface (C) arising from advective (Ψ), diffusive (D), and surface buoyancy (B_o) fluxes (adapted from Garrett et al. 1995).

$$\phi_t + \overline{\mathbf{U}} \cdot \nabla\phi = \overline{Q'b'} - \overline{\mathbf{U}'b'} \cdot \nabla\overline{b} + O(\alpha^3), \tag{A2}$$

where $O(\alpha^3)$ is used to denote the terms that are of cubic (or higher) order in perturbation quantities. Then, assuming that the flow is statistically steady ($\phi_t = 0$) and instantaneously adiabatic ($\overline{Q'b'} = 0$), and ignoring $O(\alpha^3)$, the conservation of buoyancy variance requires that

$$\overline{\mathbf{U}} \cdot \nabla\phi = -\overline{\mathbf{U}'b'} \cdot \nabla\overline{b}. \tag{A3}$$

As pointed out by McDougall and McIntosh, this means that, if the eddy buoyancy flux $\overline{\mathbf{U}'b'}$ were along mean buoyancy surfaces, then the mean flow would circulate around contours of constant buoyancy variance (i.e., $\overline{\mathbf{U}} \cdot \nabla\phi = 0$). This is not what is, in general, observed. Thus, the eddy buoyancy flux can have a component through the mean buoyancy surface (i.e., $\overline{\mathbf{U}'b'} \cdot \nabla\overline{b} \neq 0$), even if the flow is instantaneously adiabatic.

APPENDIX B

Diapycnal Transformation

Following Garrett et al. (1995), consider the control volume between the sea surface and a control surface C, and between isopycnals with buoyancy b and $b + \delta b$ (Fig. B1). Let $\Psi(b)$ represent the volume flux across the isopycnal b between the surface and C. The net diffusive buoyancy flux is denoted by D. Then, assuming steady state, the conservation of the control volume gives

$$\Psi(b) - \Psi(b + \delta b) - \left(\frac{d\Psi}{db}\right)\delta b = 0, \tag{B1}$$

whereas the conservation of buoyancy implies

$$\Psi(b)b - \Psi(b + \delta b)(b + \delta b) - \left(\frac{d\Psi}{db}\right)b\delta b + B_o\delta y + D(b) - D(b + \delta b) = 0, \tag{B2}$$

where B_o is the buoyancy flux at the surface (positive downward). Dividing the latter equation by δb and taking the limit $\delta b \rightarrow 0$, we obtain [cf. Eq. (10)]:

$$\Psi(b) = B_o(dy/db) - dD/db. \qquad \text{(B3)}$$

Thus, if the control surface bounding the isopycnals at depth is taken as the base of a well mixed surface layer and if the diapycnal diffusive flux in this layer is weak, then the diapycnal volume flux within the layer can be estimated from the flux of buoyancy at the surface.

REFERENCES

Bryan, K., and L. Lewis, 1979: A water mass model of the world ocean. *J. Geophys. Res.,* **84,** 2503–2517.

——, S. Manabe, and C. Pacanowski, 1975: A global ocean–atmosphere climate model. Part II. The oceanic circulation. *J. Phys. Oceanogr.,* **5,** 30–46.

Cerovečki, I., R. A. Plumb, and W. Heres, 2009: Eddy transport and mixing in a wind- and buoyancy-driven jet on the sphere. *J. Phys. Oceanogr.,* **39,** 1133–1149.

Danabasoglu, G., J. McWilliams, and P. Gent, 1994: The role of mesoscale tracer transport in the global ocean circulation. *Science,* **264,** 1123–1126.

——, R. Ferrari, and J. C. McWilliams, 2008: Sensitivity of an ocean general circulation model to a parameterization of near-surface eddy fluxes. *J. Climate,* **21,** 1192–1208.

Delworth, T. L., and F. Zeng, 2008: Simulated impact of altered Southern Hemisphere winds on the Atlantic meridional overturning circulation. *Geophys. Res. Lett.,* **35,** L20708, doi:10.1029/2008GL035166.

Döös, K., and D. J. Webb, 1994: The Deacon Cell and the other meridional cells of the Southern Ocean. *J. Phys. Oceanogr.,* **24,** 429–442.

——, J. Nycander, and A. C. Coward, 2008: Lagrangian decomposition of the Deacon Cell. *J. Geophys. Res.,* **113,** C07028, doi:10.1029/2007JC004351.

Drijfhout, S. S., 2005: What sets the surface eddy mass flux in the Southern Ocean? *J. Phys. Oceanogr.,* **35,** 2152–2166.

Ducet, N., P. Y. Le Traon, and G. Reverdin, 2000: Global high-resolution mapping of ocean circulation from TOPEX/Poseidon and ERS-1 and -2. *J. Geophys. Res.,* **105,** 19 477–19 498.

Dukowicz, J., and R. Smith, 1994: Implicit free-surface method for the Bryan–Cox–Semtner ocean model. *J. Geophys. Res.,* **99,** 7991–8014.

Fyfe, J. C., O. A. Saenko, K. Zickfeld, M. Eby, and A. J. Weaver, 2007: The role of poleward intensifying winds on Southern Ocean warming. *J. Climate,* **20,** 5391–5400.

Garrett, C., K. Speer, and E. Tragou, 1995: The relationship between water mass formation and the surface buoyancy flux, with application to Phillips' Red Sea model. *J. Phys. Oceanogr.,* **25,** 1696–1705.

Gent, P. R., and J. C. McWilliams, 1990: Isopycnal mixing in ocean general circulation models. *J. Phys. Oceanogr.,* **20,** 150–155.

——, J. Willebrand, T. J. McDougall, and J. C. McWilliams, 1995: Parameterizing eddy-induced tracer transports in ocean circulation models. *J. Phys. Oceanogr.,* **25,** 463–474.

Gerdes, R., C. Köberle, and J. Willebrand, 1991: The influence of numerical advection schemes on the results of ocean general circulation models. *Climate Dyn.,* **5,** 211–226.

Gnanadesikan, A., 1999: A simple predictive model for the structure of the oceanic pycnocline. *Science,* **283,** 2077–2079.

——, and Coauthors, 2006: GFDL's CM2 global coupled climate models. Part II: The baseline ocean simulation. *J. Climate,* **19,** 675–697.

Hallberg, R. W., and A. Gnanadesikan, 2006: The role of eddies in determining the structure and response of the wind-driven Southern Hemisphere overturning: Results from the Modeling Eddies in the Southern Ocean (MESO) project. *J. Phys. Oceanogr.,* **36,** 2232–2252.

Hibler, W., 1979: A dynamic thermodynamic sea ice model. *J. Phys. Oceanogr.,* **9,** 815–846.

Hirst, A. C., and T. J. McDougall, 1998: Meridional overturning and dianeutral transport in a z-coordinate ocean model including eddy-induced advection. *J. Phys. Oceanogr.,* **28,** 1205–1223.

Hughes, C. W., 2000: A theoretical reason to expect inviscid western boundary currents in realistic oceans. *Ocean Modell.,* **2,** 73–83.

Hunke, E. C., and J. K. Dukowicz, 1997: An elastic–viscous–plastic model for sea ice dynamics. *J. Phys. Oceanogr.,* **27,** 1849–1867.

Iudicone, D., G. Madec, and T. J. McDougall, 2008: Water-mass transformations in a neutral density framework and the key role of light penetration. *J. Phys. Oceanogr.,* **38,** 1357–1376.

Jochum, M., G. Danabasoglu, M. Holland, Y. Kwon, and W. Large, 2008: Ocean viscosity and climate. *J. Geophys. Res.,* **113,** C06017, doi:10.1029/2007JC004515.

Johnson, H. L., and D. P. Marshall, 2004: Global teleconnections of meridional overturning circulation anomalies. *J. Phys. Oceanogr.,* **34,** 1702–1722.

Karsten, R., H. Jones, and J. Marshall, 2002: The role of eddy transfer in setting the stratification and transport of a circumpolar current. *J. Phys. Oceanogr.,* **32,** 39–54.

Kistler, R., and Coauthors, 2001: The NCEP–NCAR 50-Year Reanalysis: Monthly means CD-ROM and documentation. *Bull. Amer. Meteor. Soc.,* **82,** 247–267.

Lee, M.-M., A. J. G. Nurser, A. C. Coward, and B. A. de Cuevas, 2007: Eddy advective and diffusive transports of heat and salt in the Southern Ocean. *J. Phys. Oceanogr.,* **37,** 1376–1393.

Levitus, S., and T. P. Boyer, 1994: *Temperature*. Vol. 4, *World Ocean Atlas 1994,* NOAA Atlas Nesdis 4, 117 pp.

——, R. Burgett, and T. P. Boyer, 1994: *Salinity*. Vol. 3, *World Ocean Atlas 1994,* NOAA Atlas Nesdis 3, 99 pp.

Marshall, J., and T. Radko, 2003: Residual-mean solutions for the Antarctic Circumpolar Current and its associated overturning circulation. *J. Phys. Oceanogr.,* **33,** 2341–2354.

——, and ——, 2006: A model of the upper branch of the meridional overturning circulation of the Southern Ocean. *Prog. Oceanogr.,* **70,** 331–345.

Matthews, H. D., A. J. Weaver, M. Eby, and K. J. Meissner, 2003: Radiative forcing of climate by historical land cover change. *Geophys. Res. Lett.,* **30,** 1055, doi:10.1029/2002GL016098.

McDougall, T. J., and P. C. McIntosh, 1996: The temporal-residual-mean velocity. Part I: Derivation and the scalar conservation equations. *J. Phys. Oceanogr.,* **26,** 2653–2665.

——, and ——, 2001: The temporal-residual-mean velocity. Part II: Isopycnal interpretation and the tracer momentum equations. *J. Phys. Oceanogr.,* **31,** 1222–1246.

——, P. R. Gent, and S. Drijfhout, 2007: Comment on "dynamical model of mesoscales in z-coordinates" and "the effect of mesoscales on the tracer equation in z-coordinates OGCMs" by V. M. Canuto and M. S. Dubovikov. *Ocean Modell.,* **17,** 163–171.

McIntosh, P. C., and T. J. McDougall, 1996: Isopycnal averaging and the residual mean circulation. *J. Phys. Oceanogr.,* **26,** 1655–1660.

Pacanowski, R., 1995: MOM 2 documentation, user's guide, and reference manual. GFDL Ocean Group Tech. Rep. 3, NOAA/GFDL, 232 pp.

Plumb, R. A., and R. Ferrari, 2005: Transformed Eulerian-mean theory. Part I: Nonquasigeostrophic theory for eddies on a zonal-mean flow. *J. Phys. Oceanogr.,* **35,** 165–174.

Radko, T., and J. Marshall, 2004: Eddy-induced diapycnal fluxes and their role in the maintenance of the thermocline. *J. Phys. Oceanogr.,* **34,** 372–383.

Roberts, J., and Coauthors, 2004: Impact of an eddy-permitting ocean resolution on control and climate change simulations with a global coupled GCM. *J. Climate,* **17,** 3–20.

Saenko, O. A., 2007: Projected strengthening of the Southern Ocean winds: Some implications for the deep ocean circulation. *Ocean Circulation: Mechanisms and Impacts, Geophys. Monogr.,* Vol. 173, Amer. Geophys. Union, 365–382.

——, J. C. Fyfe, and M. H. England, 2005: On the response of the oceanic wind-driven circulation to CO_2 increase. *Climate Dyn.,* **25,** 415–426.

Semtner, A. J., and R. M. Chervin, 1988: A simulation of the global ocean circulation with resolved eddies. *J. Geophys. Res.,* **93,** 15 502–15 522.

Speer, K., E. Guilyardi, and G. Madec, 2000a: Southern Ocean transformation in a coupled model with and without eddy mass fluxes. *Tellus,* **52A,** 554–565.

——, S. R. Rintoul, and B. Sloyan, 2000b: The diabatic deacon cell. *J. Phys. Oceanogr.,* **30,** 3212–3222.

Toggweiler, J. R., and J. Russell, 2008: Ocean circulation in a warming climate. *Nature,* **451,** 286–288.

Treguier, A. M., I. M. Held, and V. D. Larichev, 1997: Parameterization of quasigeostrophic eddies in primitive equation ocean models. *J. Phys. Oceanogr.,* **27,** 567–580.

——, M. H. England, S. R. Rintoul, G. Madec, J. Le Sommer, and J. M. Molines, 2007: Southern Ocean overturning across streamlines in an eddying simulation of the Antarctic Circumpolar Current. *Ocean Science,* **3,** 491–507.

Walin, G., 1982: On the relation between sea-surface heat flow and thermal circulation in the ocean. *Tellus,* **34,** 187–195.

Weaver, A. J., and Coauthors, 2001: The UVic Earth System Climate Model: Model description, climatology and application to past, present and future climates. *Atmos.–Ocean,* **39,** 361–428.

Webb, D. J., and Coauthors, 1991: An eddy-resolving model of the Southern Ocean. *EOS, Trans. Amer. Geophys. Union,* **72,** 169–174.

Wiebe, E. C., and A. J. Weaver, 1999: On the sensitivity of global warming experiments to the parametrisation of sub-grid scale ocean mixing. *Climate Dyn.,* **15,** 875–893.

Wunsch, C., 2007: The past and future ocean circulation from a contemporary perspective. *Ocean Circulation: Mechanisms and Impacts, Geophys. Monogr.,* Vol. 173, Amer. Geophys. Union, 53–74.

Zickfeld, K., J. C. Fyfe, O. C. Saenko, M. Eby, and A. J. Weaver, 2007: Response of the global carbon cycle to human-induced changes in Southern Hemisphere winds. *Geophys. Res. Lett.,* **34,** L12712, doi:10.1029/2006GL028797.